Frequency- and circuit- specific effects of septohippocampal deep brain stimulation in mice as measured by functional ultrasound imaging.

Authors

Lindsey M. Crown, PhD,[*2] Kofi Agyeman, MS[*5], Wooseong Choi, BS,[*1] Nancy Zepeda, BS,[1] Steven J. Siegel, MD, PhD,[2] Charles Liu, MD, PhD,[§1,3,4,6] Vasileios Christopoulos, PhD,[§3,5,7] Darrin J. Lee, MD, PhD[§1,2,3,4,6]

Affiliations

[1]Department of Neurological Surgery, Keck School of Medicine, University of Southern California, Los Angeles, CA, USA

[2]Department of Psychiatry and Behavioral Sciences, Keck School of Medicine, University of Southern California, Los Angeles, CA, 90033, USA

[3]Neurorestoration Center, Keck School of Medicine, University of Southern California, Los Angeles, CA, USA

[4]Department of Biomedical Engineering, Viterbi School of Engineering, University of Southern California, Los Angeles, CA, USA

[5]Department of Bioengineering, University of California Riverside, Riverside, CA, USA

[6]Rancho Los Amigos National Rehabilitation Center, Downey, CA, USA

[7]Neuroscience Graduate Program, University of California Riverside, Riverside, CA, USA

[*] These authors contributed equally

[§] These authors jointly supervised this work (Correspondence)

Significance Statement

Deep brain stimulation (DBS) is a well-established treatment for neurological and neuropsychiatric diseases, yet it's mechanism of action remains unknown. We recently demonstrated that medial septal nucleus (MSN) DBS improves spatial memory in rodents treated with the NMDA antagonist MK-801, a drug known to mimic cognitive impairment in schizophrenia. Here we utilize functional ultrasound imaging (fUSI) in mice to visualize the effects of MSN DBS on cerebral blood volume (CBV) following saline or MK-801 administration. We find that theta frequency-specific (7.7Hz) MSN DBS restored MK-801-induced CBV reductions within the septohippocampal circuit (i.e., hippocampus) after stimulation offset. These results demonstrate that MSN stimulation drives circuit-specific neurovascular activity and may ultimately improve cognitive function in diseases with NMDA hypofunction, such as schizophrenia.

Abstract

Deep brain stimulation (DBS) has shown remarkable success in treating neurological and psychiatric disorders such as Parkinson's disease, essential tremor, dystonia, epilepsy, and obsessive-compulsive disorder. Despite this success, the underlying mechanism of action remains unknown. DBS is now being explored as a means to improve cognition and functional outcomes in other psychiatric conditions, such as those characterized by reduced N-methyl-D-aspartate (NMDA) function (i.e. schizophrenia). While most DBS treatments for movement disorders require continuous stimulation, there is evidence that intermittent stimulation in cognitive and psychiatric

conditions may have persisting effects beyond the period of stimulation. This suggests that the effects of DBS on brain activity last beyond the time of its acute electrical effects, necessitating a broader exploration of how neuromodulation alters brain networks. In this study, we utilize a novel technology, functional ultrasound imaging (fUSI), to characterize the cerebrovascular impact of medial septal nucleus (MSN) DBS under conditions of NMDA antagonism (pharmacologically using Dizocilpine [MK-801]) in anesthetized male mice. Imaging from a sagittal plane across a variety of brain regions, we find that MSN theta-frequency (7.7Hz) DBS had a larger effect on hippocampal cerebral blood volume (CBV) after stimulation offset. This was observed following an intraperitoneal (i.p.) injection of either saline vehicle or MK-801 (1 mg/kg). This effect was not present using standard high frequency DBS stimulation parameters (i.e. gamma [100Hz]). These results indicate the MSN DBS increases circuit-specific hippocampal neurovascular activity in a frequency-dependent manner and does so in manner that continues beyond the period of electrical stimulation.

Introduction

There is growing interest in utilizing neuromodulation to treat cognitive impairment associated with neurological and psychiatric disorders. Many of these disorders involve aberrant electrophysiology and cerebral blood perfusion [1,2]. Recent evidence demonstrates that electrical neuromodulation can improve functional outcomes [3,4]. Particularly, deep brain stimulation (DBS) has shown remarkable success in treating neurological diseases such as movement disorders and epilepsy, and there is increasing evidence for its efficacy in cognitive and psychiatric conditions.

Despite this growing utility, the underlying mechanism of DBS for cognitive outcomes remains largely unknown. Pre-clinical studies have been hindered by technological limitations, such as the inability to record electrical brain activity during stimulation and the low spatial resolution of electrographic measures. Functional ultrasound imaging (fUSI) is a relatively new technology that enables large-scale estimates of neural activity through measures of cerebral blood volume (CBV). fUSI provides a unique combination of high spatiotemporal resolution (~100 μm^3, up to 10 ms) and high sensitivity to slow blood flow (~1 mm/s velocity) across a large field of view. In fact, fUSI has already been proven to be an effective tool for imaging large-scale brain activity and pharmacodynamics [5–8]. As such, it is well-positioned to improve our understanding of the impact of DBS on large-scale brain networks during and immediately following stimulation.

In many disorders, cognitive dysfunction is accompanied by altered septohippocampal network activity. For instance, neural oscillatory patterns within the septohippocampal network, such as gamma- and theta-band activity, are

characteristically altered in disorders such as schizophrenia and Alzheimer's disease and are often correlated with impaired memory [1,9–11]. Alterations in specific neurotransmitter signal transduction pathways also play an important role in modulating neural oscillatory activity. In particular, the glutamatergic *N*-methyl-D-aspartate (NMDA) receptor is crucial to regulating hippocampal theta and gamma oscillations and is the predominant molecular control for synaptic plasticity and memory function [12–14] As such, pharmacologic NMDA receptor antagonism (i.e. via MK-801) results in characteristic changes to neural oscillatory patterns and memory dysfunction [15–19].

The medial septal nucleus (MSN) is a key structure in the septohippocampal network that modulates sensory-motor processing and acts as a "pacemaker" for hippocampal theta oscillations via dense glutamatergic, cholinergic, and GABAergic projections to the hippocampus [20,21]. This makes the MSN a promising target for DBS in cognitive disorders involving memory impairments [22]. Our recent work as well as that of others suggest that modulating the septohippocampal network via MSN DBS can restore cognitive impairment and memory dysfunction in preclinical models of epilepsy, traumatic brain injury, Alzheimer's disease, and schizophrenia [22–27].

In the current study, we utilize fUSI to characterize the effects of MK-801 on CBV in the septohippocampal network (Fig. 1A) including the MSN, hippocampus, and medial prefrontal cortex (mPFC). Within the same sagittal plane, we also image CBV changes (ΔCBV) to regions of interest (ROIs) outside this network including the striatum, thalamus, hypothalamus, and pallidum. Additionally, we determine the effect of direct MSN stimulation on blood flow in these areas using two distinct frequencies, theta (7.7Hz) and gamma (100Hz). Finally, we test the hypothesis that MSN theta-

frequency-specific stimulation can improve blood flow under conditions of reduced NMDA function.

Figure 1

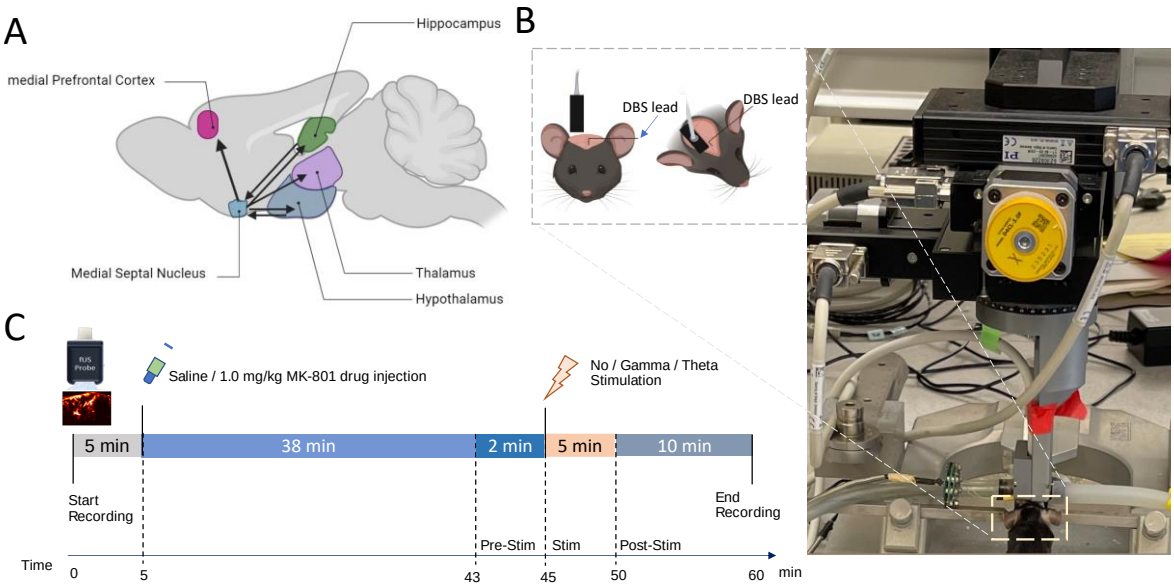

Figure 1. Experimental setup and fUSI recording protocol. A) Schematic illustration of connectivity between the MSN and ROIs. Arrowheads represent axonal projections to and/or from MSN. **B)** Experimental set-up showing the anesthetized mouse in a stereotaxic frame under the Iconeous One motorized probe mount. DBS stimulating electrodes were implanted on the left hemisphere and a sagittal plane of the right hemisphere was imaged**. C)** Diagram of the protocol for 60 minutes of continuous fUSI acquisition consisting of saline or 1.0 mg/kg MK-801 drug injection (at the 5-minute mark) and 5 minutes of gamma- or theta-frequency DBS (at the 45-minute mark).

Materials and Methods

Animals and surgical procedures

82 male 8–12-week-old C57BL/6 mice (Charles River Laboratories; Hollister, CA) were used in this study. fUSI data from two animals were excluded due to extreme values (Grubbs test for outliers, 98th percentile of all maximum change in pD intensities) that did not appear physiological [28,29]. The animals were divided into two main groups: saline vehicle control (n=46) and MK-801 drug-administered (n=34). Each group was then sub-divided into three categories: no stimulation (saline: n=14; MK-801: n=10), theta stimulation (saline: n=16, MK-801: n=12), and gamma stimulation (saline: n=14, MK-801: n=14).

Mice were anaesthetized with 5% isoflurane in O_2/N_2O (1:2) carrier gas and then maintained at a constant rate (1.5- 2%) through surgery and data acquisition. Body temperature was kept constant throughout recordings by placing animals on an electric heating pad. Hair was removed from the mouse's head for fUSI using a commercially available depilatory cream (Nair, Pharmapacks).

To implant DBS electrodes, mice were head-fixed in a stereotaxic frame (David Kopf instruments, Tujunga, CA) and a midline incision of the scalp was made to expose the skull. A 2mm burr hole was then drilled to implant bipolar stimulating electrodes (E363T/2/SPC ELEC .008"/.2MM, Plastics One Inc., Roanoke, VA) targeting the MSN (AP: +0.7mm, ML: -0.9mm, from bregma. Z: -4.39mm at 11.8 degrees) from the left hemisphere. Prior to implantation, the electrodes were connected to an electronic interface board (Neuralynx Inc., Bozeman, MT) and bent at 4.5mm from the tip to maximize the proximity of the fUSI probe to the skull. All procedures were approved by

the University of Southern California, Institutional Animal Care and Use Committee (IACUC #21006).

Histology

Mice were euthanized immediately after the fUSI recording by isoflurane overdose followed by transcardial perfusion using 50 mL of 0.1M sodium phosphate buffer saline (PBS) and 50 mL of 4% paraformaldehyde. Brains were harvested and stored in phosphate buffered saline at 4˚C. To confirm electrode positioning within the MSN, coronal sections were cut at 100µm thickness with a vibratome (Leica VT 1200; Leica Biosystems, Buffalo Grove, IL) and then Nissl stained with Cresyl Violet (Fig. 2A,B).

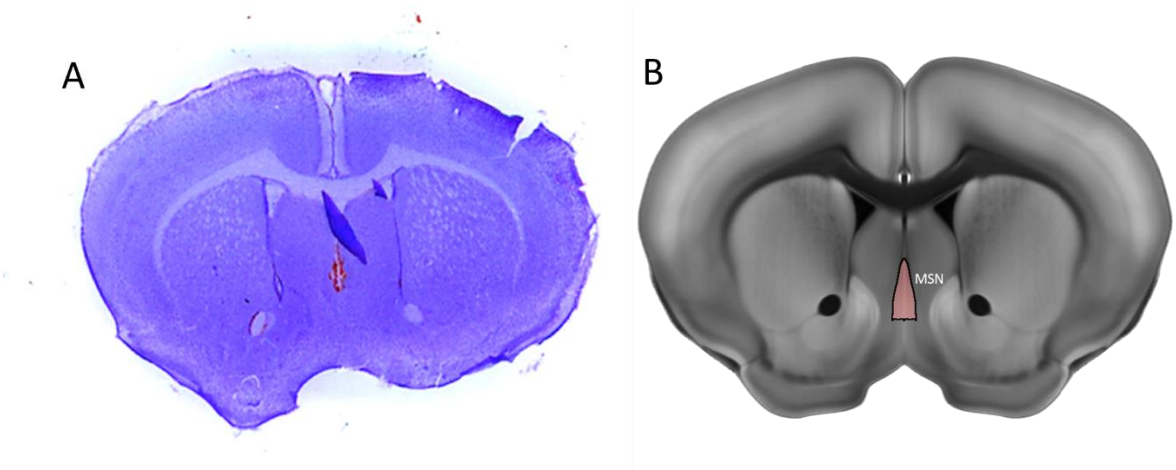

Figure 2. Histological mapping of electrode placement in the MSN. A) Representative Nissl stain of the mouse brain with a blood mark indicating the electrode placement **B)** Annotation of the MSN from the Allen Reference Atlas – Mouse Brain in the same slice position as A.

Data Acquisition

fUSI data were acquired using the *Iconeus One* system (Iconeus, Paris, France). Image acquisition was performed using 128-channel linear ultrasound transducer array, with 15 MHz center frequency and 0.1 mm pitch. This technique enables a large field of view (12.8 mm width, 10 mm depth and 400 µm plane thickness) while maintaining high spatial resolution (100 µm x 100 µm in-plane). The transducer was placed on the intact skull and skin along a sagittal plane on the right side, contralateral to the implanted stimulating electrodes (Fig. 1B). A 60-minute continuous fUSI signal acquisition protocol was employed (Fig. 1C), after 5 minutes, an intraperitoneal (i.p) injection of either 0.2cc of saline or MK-801 (1mg/kg) was given. At the 45-minute mark, mice received either 5 minutes theta (7.7Hz), 5 minutes gamma (100Hz), or no stimulation in the MSN, followed by an additional 10 minutes of fUSI recording (Fig. 1B). This timepoint was chosen as the maximal concentration of MK-801 in the brain when given systemically occurs 40-60 minutes after injection [30]. The MSN was electrically stimulated at gamma and theta under the following parameters: 100 msec square wave pulse width, and current of 80µA using a STG 4008 (Multi-Channel Systems, Baden-Württemberg, Germany). These parameters were chosen because they have previously been shown to improve memory function in animal models of spatial memory impairment [23,25,27].

The target image plane was determined by co-registering a 3D whole-brain fUSI image of each mouse with a standard Allen Mouse Common Coordinates Framework brain atlas utilizing dedicated software available with the Iconeus One system (Fig. 3A)

[31]. The probe was fixed steadily throughout experiments on a motorized system with the field of view (FOV) transverse and intersecting the co-registered sagittal plane. Images were obtained from 200 compounded frames acquired with a 500Hz frame rate, using 11 tilted plane waves separated by 2° (from -10° to +10° increment by 2°). These were acquired at a 5500Hz pulse repetition frequency (PRF) using a real-time continuous acquisition of successive blocks of 400ms (with 600ms pause between pulses) of compounded plane wave images.

Data analysis

Data pre-processing:

The Iconeus One acquisition system generates power Doppler (pD) images pre-processed with built-in phase-correlation based sub-pixel motion registration and singular-value-decomposition (SVD) based clutter filtering algorithms [32]. These algorithms were used to separate tissue signal from blood signal to obtain pD images (Fig. 3B). To correct potential physiological and motion artifacts, we adopted rigid motion correction techniques that have successfully been used in fUSI and other neuroimaging studies [33–35]. These were combined with high frequency filtering algorithms to eliminate noise artifacts. We employed a low-pass filter with normalized passband frequency of 0.02 Hz, with a stopband attenuation of 60 dB that compensates for delay introduced by the filter, to remove high-frequency fluctuations in the pD signals.

Effects of MK-801 on CBV

We investigated the temporal effects of intraperitoneal MK-801 administration on the septohippocampal circuit (hippocampus, mPFC) and surrounding regions (striatum, pallidum, thalamus, hypothalamus). To do so, we generated event-related average (ERA) time course curves of the CBV changes (ΔCBV) as a percentage change of the pD signal from baseline activity for the selected ROIs. The average pD signal from 2 minutes prior to the saline or drug injection was used as the baseline. We utilized a repeated measures analysis of variance (rmANOVA) to assess the effects and interactions between drug (saline and MK801) and ROI factors over time. We fitted a repeated measures '*within-design'* model to the CBV percentage change signals over 42-min interval (including 2 minutes just before the drug injection and the 40 minutes after injection) for each mouse and ROI for the rmANOVA analysis. To further quantify the relative differences in ΔCBV between saline-vehicle and MK-801-treated mice in various ROIs, we used the last 2 minutes of recordings to compute the mean effects-size differences in ΔCBVs and the 95% confidence interval of the effect size (if 95% confidence interval contains zero, then the effect is not significant at the 0.05 level) in each ROI. We also computed the Cohen's *d* value in each ROI as a measure of the drug effect size that describes the standardized difference between the means of ΔCBVs in the two groups of animals [36]. A Cohen's d value of 0.2 represents a small effect size, 0.5 represents a moderate effect size, 0.8 represents a large size and greater than 0.8 represents a very large size.

Effects of MSN DBS during stimulation on brain hemodynamics

We computed the ΔCBV for each ROI to investigate effects of MSN theta- and gamma- frequency stimulation on the cerebral hemodynamics following saline control or MK-801 injection. We observed ERA time-series of the ΔCBV of each selected ROI relative to the average pD signal acquired 2 minutes prior to stimulation onset to visualize the temporal dynamics of DBS effects to CBVs of the ROIs. We utilized a three-way rmANOVA to assess the effects and interactions between drug (saline and MK801), stimulation (gamma, theta, no-stimulation) and ROI factors across time during the stimulation process. Here, we fit a repeated measures '*within-design'* model to the ΔCBV signals over the 7-min period (including 2 minutes prior to stimulation, 5 minutes during stimulation) for each animal and ROI. Subsequently, we computed the mean effects-size differences in ΔCBVs, the 95% confidence interval of the effect size, and the Cohen's *d* value in each ROI as a measure of the stimulation effect size. We measured the mean ΔCBVs during stimulation in theta [saline: n=16, MK-801: n=12], gamma [saline: n=14, MK-801: n=14], and no-stimulation [saline: n=14; MK-801: n=10] animal groups. The mean ΔCBVs were calculated utilizing the last 2 minutes of pD signal during stimulation across animals in each of the three stimulation categories.

Effects of MSN DBS after stimulation offset on brain hemodynamics

We are also interested in assessing the effects of MSN DBS after stimulation offset. To do so, we repeated the same analysis described above, but we used the 10 minutes of pD signal after stimulation offset, plus 2 minutes prior to stimulation onset as a baseline. The mean ΔCBVs were calculated utilizing the last 2 minutes of pD signal after

stimulation offset across animals in each of the three stimulation categories. Our goal is to identify whether MSN DBS causes persistent and delayed changes in CBVs within and/or outside the septohippocampal network.

Statistical analysis of drug and stimulation effects on ΔCBVs

All the analysis was performed using Matlab Version 9.13.0.2193358 (R2022b). We assessed the drug and stimulation effects and interactions utilizing the Matlab functions *'fitrm'* and *'ranova'* for the repeated measures model fitting and the rmANOVA respectively. We utilized the Greenhouse-Geisser approximation to correct for the possibility of non-compound symmetry (same variance in means and shared common correlation in paired responses) in the ROI-time series assessed. The mean effect-size differences and the *Cohen's d* values for the mean difference in ΔCBVs between saline and MK801, as well as the between no-stimulation-gamma, no-stimulation-theta, and gamma-theta were computed with the *'meanEffectSize'* Matlab function.

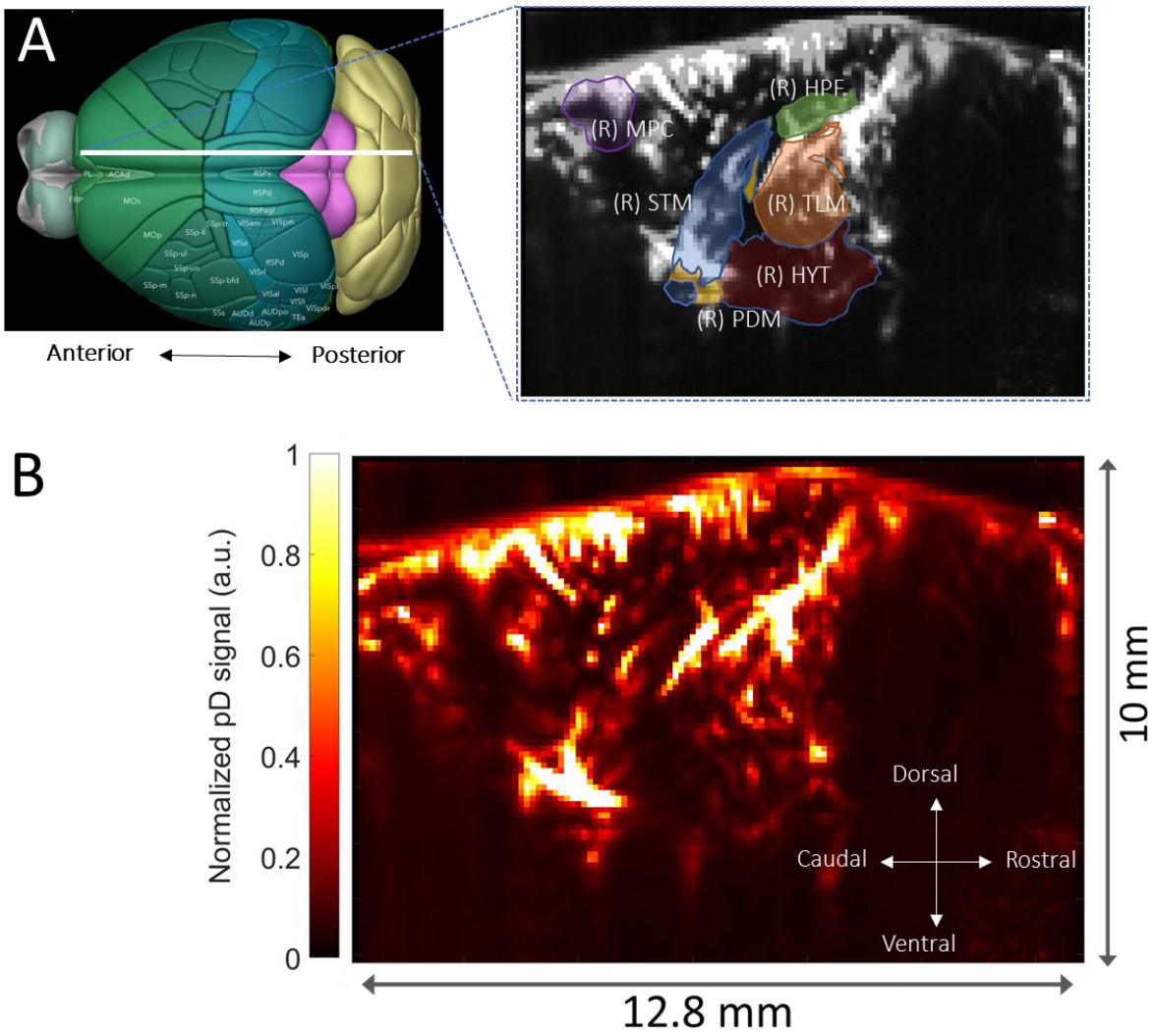

Figure 3. Functional ultrasound imaging (fUSI) of the mouse brain. A) 3D mouse brain model with fUSI probe positioning (white bar) and ROIs – hippocampus (HPF), medial prefrontal cortex (mPFC), hypothalamus (HYT), thalamus (TLM), pallidum (PDM), and striatum (STM), superimposed onto a mean grayscale fUSI vascular map of the sagittal mouse brain. **B)** pD image of cerebral blood volume (CBV) in a sagittal plane (max-min normalized relative scale).

Results

NMDA antagonist MK-801 reduced blood perfusion

We analyzed 40 minutes of pD signal from the septohippocampal circuit (hippocampus, mPFC) as well as surrounding structures (hypothalamus, thalamus, pallidum, and striatum) to assess the effects of MK-801 on cerebral hemodynamics (Fig. 1A). We quantified changes in CBV (ΔCBV) as a percent change relative to baseline activity (average of 2 minutes pD signal acquired prior to drug injection). A repeated measures ANOVA (factors treatment × ROI; where treatment is saline vs. MK-801 and ROI is the 6 recorded brain areas) revealed that there was a statistically significant effect over time ($F(2519, 56406) = 8.76$, $p = 6.3\ e\text{-}5$) after Greenhouse-Geiser approximation correction. To quantify the effect of MK-801 on CBV, we computed the percentage change (i.e., ΔCBV) relative to baseline using the last two minutes before stimulation onset (38-40 minutes after drug injection) and found a reduction of ΔCBV (mean ± SEM) in the hippocampus (-3.6 ± 1.1 %), mPFC (-4.1 ± 0.61 %), hypothalamus (-1.0 ± 0.2 %), pallidum (-1.5 ± 0.4 %), striatum (-1.7 ± 0.3 %), and thalamus (-3.0 ± 0.5 %). For saline-treated animals these values were: hippocampus (-0.7 ± 0.6 %), mPFC (-0.1 ± 0.2 %), hypothalamus (-0.7 ± 0.6 %), pallidum (0.9 ± 0.4 %), striatum (-0.3 ± 0.4 %), and thalamus (0.2 ± 0.4 %) (Fig. 4A-F, radar chart insert). The mean effect-size difference in ΔCBVs and Cohen's d analysis comparing mean ΔCBV induced by saline and MK-801 over a 2-minute interval (38 – 40 minutes post-drug injection), revealed that MK-801 induces greater decreases in CBV than saline control in all ROIs

investigated (Fig. 4A-F, radar chart insert) - i.e., mPFC (ΔCBV mean difference between saline and MK-801 animals ± confidence, Cohen's d; 3.96 ± 0.38 %, d= 0.42), thalamus (3.17 ± 0.23 %, d= 0.55), hippocampus (2.82 ± 0.42 %, d= 0.27), pallidum (2.42 ± 0.20 %, d= 0.49), hypothalamus (1.72 ± 0.12 %, d= 0.59) and striatum (1.33 ± 0.18 %, d= 0.29). Together, these results indicate that MK-801 reduces CBV both within and outside of the septohippocampal network.

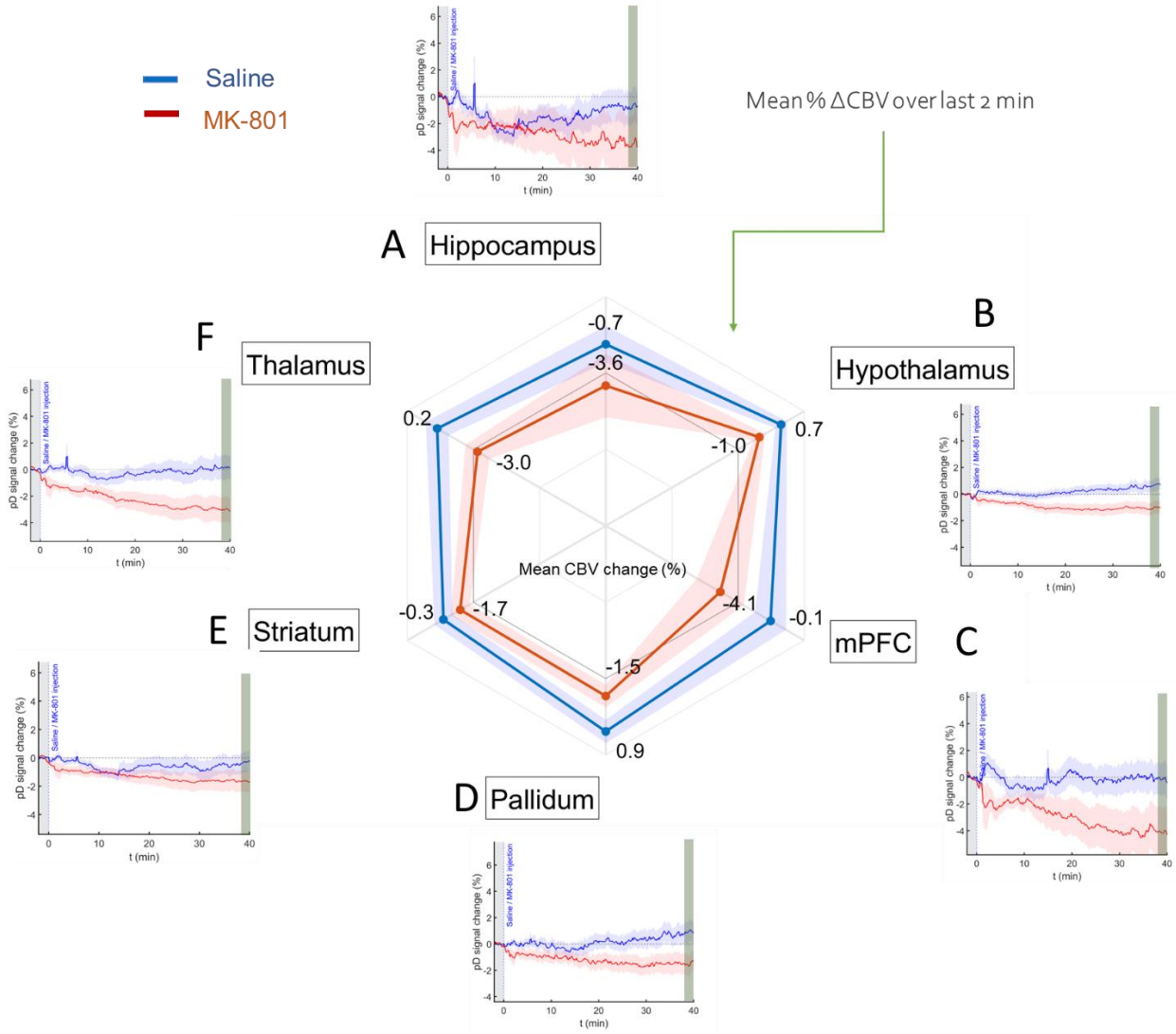

Figure 4. Event related average (ERA) temporal course curves prior to stimulation onset and mean ΔCBVs during the last 2 minutes in saline and MK-801 treated animals. A – F) Temporal course (42 minutes) of ΔCBV relative to baseline (2-minute average pD signal before saline or MK-801 drug injection) in the A) hippocampus, B) hypothalamus, C) mPFC, D) pallidum, E) striatum, and F) thalamus after saline [blue] and 1.0 mg/kg MK-801 [red] injection. The radar chart insert shows MK-801-induced decreases in CBV in all ROIs compared to saline over the last 2 minutes interval from 38-40 minutes post injection.

<u>MSN stimulation increases CBV in saline control animals in a frequency- and region-dependent manner.</u>

We assessed whether theta- and gamma-frequency MSN stimulation has disparate impacts on CBV measures in saline-treated control mice. ERAs of ΔCBV reflect the temporal responses to theta, gamma, and no stimulation during and post stimulation time periods (Fig. 5, 6). A three-way repeated measures ANOVA (factors, treatment × ROI × DBS; where treatment is saline vs. MK-801, ROI is the 6 recorded brain areas, and DBS is theta frequency vs. gamma frequency vs no DBS) was utilized to examine the effects and interactions of drug, stimulation, and ROIs during the 5 minutes period after onset of MSN stimulation. The two-minute baseline period pre-stimulation was included in the analysis. We found significant effects of drug over time ($F(419, 186036) = 7.35$, $p = 1.85\ e\text{-}8$), stimulation over time ($F(823, 186036) = 2.71$, $p = 7.20\ e\text{-}4$), as well as, interaction of drug and stimulation over time ($F(838, 186036) =$

1.96, p = 1.95 e-2) during the 5 minutes stimulation interval, after Greenhouse-Geisser approximation correction. To further quantify the effects of DBS, we computed the mean ΔCBV in the last 2 minutes during stimulation across animals in each stimulation category and compared the mean-effect size differences in ΔCBVs between no stimulation and stimulation in each ROI. We found that MSN theta stimulation increased CBV compared to no-stimulation only in the mPFC (mean ΔCBV difference between theta- and no-stimulation ± confidence, Cohen's d; 0.82 ± 0.12 %, d= 0.45) and hippocampus (0.39 ± 0.12 %, d= 0.21). For the rest on ROIs the effect size magnitude was either very small (i.e., Cohen's d <0.08) or theta-frequency stimulation caused further reduction in CBVs compared to no-stimulation. On the other hand, MSN gamma stimulation caused increases in CBV compared to no-stimulation in the mPFC (0.60 ± 0.11 %, d= 0.36), pallidum (0.38 ± 0.09 %, d= 0.30) and striatum (0.22 ± 0.06 %, d= 0.26). For the rest of the ROIs the effect size magnitude was either very small (i.e., Cohen's d < 0.095) or gamma-frequency stimulation resulted in further reduction in CBVs compared to no-stimulation. When comparing the ΔCBV induced by the theta and gamma stimulation in mPFC – the only ROI that exhibited moderate effect on both types of stimulations – we found very small effect size on ΔCBV between the two types of stimulations (mean ΔCBV differences between theta- and gamma-stimulation ± confidence, Cohen's d; 0.22 ± 0.10, d= 0.14).

The next step was to assess the effects of DBS after stimulation offset (i.e., post-stimulation). To do so, we conducted a three-way repeated measures ANOVA (factors, treatment × ROI × DBS; where treatment is saline vs. MK-801, ROI is the 6 recorded

brain areas, and DBS is theta frequency vs. gamma frequency vs no DBS) over the 10 minutes period after the offset of MSN stimulation. We found significant effects of drug over time ($F(1019, 452436) = 5.28$, $p = 1.27\ e\text{-}4$), stimulation over time ($F(2038, 452436) = 3.67$, $p = 1.17\ e\text{-}4$), as well as, interaction of drug and stimulation over time ($F(2038, 186036) = 3.09$, $p = 9.40\ e\text{-}4$), after Greenhouse-Geisser approximation correction, across the 10 minutes post-stimulation interval. We further quantified the post-effects of DBS by computing the mean ΔCBV in the last 2 minutes of the acquisition – i.e., 8-10 minutes post-stimulation and comparing the mean-effect size differences on ΔCBV between no stimulation and stimulation in each ROI. The results showed that MSN theta stimulation causes increases in CBV compared to no-stimulation in the hippocampus (mean ΔCBV differences between theta- and no-stimulation ± confidence, Cohen's d; 1.30 ± 0.21, d= 0.42), mPFC (1.20 ± 0.22 %, d= 0.37) and thalamus (0.97 ± 0.11 %, d= 0.58) (Fig. 6A, F – radar chart). On the other hand, MSN gamma stimulation resulted in an increase in CBV compared to no stimulation in the mPFC (2.01 ± 0.22 %, d= 0.60), striatum (0.77 ± 0.14 %, d= 0.37) and pallidum (0.61 ± 0.16 %, d= 0.25). When comparing the differences in ΔCBVs induced by theta and gamma stimulation in the mPFC – the only ROI that exhibited medium to moderate effect on both types of stimulations – we found that gamma induces higher ΔCBV than theta stimulation with medium effect size difference (mean ΔCBV differences between gamma- and theta-stimulation ± confidence, Cohen's d; 0.81 ± 0.17, d= 0.31).

Theta-frequency stimulation elicits stronger CBV increases than gamma-frequency stimulation in MK-801 treated animals.

Recently, our group showed that theta, but not gamma frequency DBS of the MSN improves spatial memory in MK-801 treated rats [27]. Therefore, we sought to determine if MSN theta and gamma frequency stimulation had differing impacts on neurovascular activity measures within memory-associated regions including the mPFC and hippocampus as well as neighboring regions outside the septohippocampal network (striatum, pallidum, thalamus, hypothalamus) following MK-801 drug-administration. Again, we assessed the mean effect-size differences in ΔCBV between MSN theta-, gamma-, and no-stimulation in each of the selected ROIs, relative to 2 minutes of pD signal recordings just prior to stimulation onset. The analysis was performed after repeated measures ANOVA over the stimulation and post-stimulation time intervals to examine the effects and interactions of drug, stimulation, and ROI (results presented in previous section). Fig. 7 and 8 display the ERA curves for ROIs in response to theta, gamma, and no DBS during and post stimulation periods in the MK-801 group. We found that MSN theta stimulation in the MK-801 treated group caused increased ΔCBV with respect to no-stimulation group with medium to large effect size in all ROIs except mPFC – i.e., hippocampus (mean ΔCBV differences between theta- and no-stimulation ± confidence, Cohen's d; 2.01 ± 0.20 %, d= 0.78), thalamus (0.49 ± 0.07 %, d= 0.54), pallidum (0.36 ± 0.07 %, d= 0.43), striatum (0.18 ± 0.04 %, d= 0.31) and hypothalamus (0.14 ± 0.04 %, d= 0.30) (Fig. 7). Intriguingly, we only found a medium effect-size increase in ΔCBV for the pallidum (0.60 ± 0.08 %, d= 0.53) and striatum (0.23 ± 0.05 %,

d= 0.38) between MSN gamma- stimulation and no-stimulation groups, during the stimulation period. For the rest of the ROIs, the effect-size was very small.

Importantly, we found that ΔCBV increased in theta- relative to no-stimulation animals after stimulation offset with medium to larger effects in the pallidum (1.26 ± 0.15 %, d=0.66), hippocampus (2.8 ± 0.37 %, d=0.60) and thalamus (1.24 ± 0.17 %, d= 0.57) and small to medium effects in the striatum (0.50 ± 0.13 %, d= 0.31), hypothalamus (0.21 ± 0.06 %, d= 0.28) and mPFC (0.64 ± 0.22 %, d= 0.22) (Fig. 8). Importantly, we found only small to medium effects of gamma MSN stimulation on ΔCBV in the pallidum, relative to stimulation animals, and after stimulation offset (mean ΔCBV differences between gamna- and no-stimulation ± confidence, Cohen's d; 0.66 ± 0.13 %, d=0.39) (Fig. 8). For the rest of the ROIs, the effect-size was either very small (i.e., Cohen's d < 0.1 in hippocampus, striatum and thalamus) or gamma-frequency stimulation resulted in further CBV reduction (i.e., in hypothalamus and mPFC) compared to no-stimulation.

Additionally, our results showed medium or large mean effect-size differences in ΔCBVs between the theta and gamma stimulated MK801 groups after stimulation offset in the hippocampus (2.67 ± 0.28 %, d= 0.70), mPFC (1.83 ± 0.23 %, d= 0.59), and thalamus (1.15 ± 0.14 %, d= 0.56) (Fig. 8). Together these results demonstrate that theta-frequency stimulation elicits the strongest CBV response in MK-801-treated mice in the hippocampus and pallidum, while gamma stimulation had almost no effect on hippocampal CBV (Cohen's d = 0.03) and decreased CBV in the mPFC compared to no-stimulation mice.

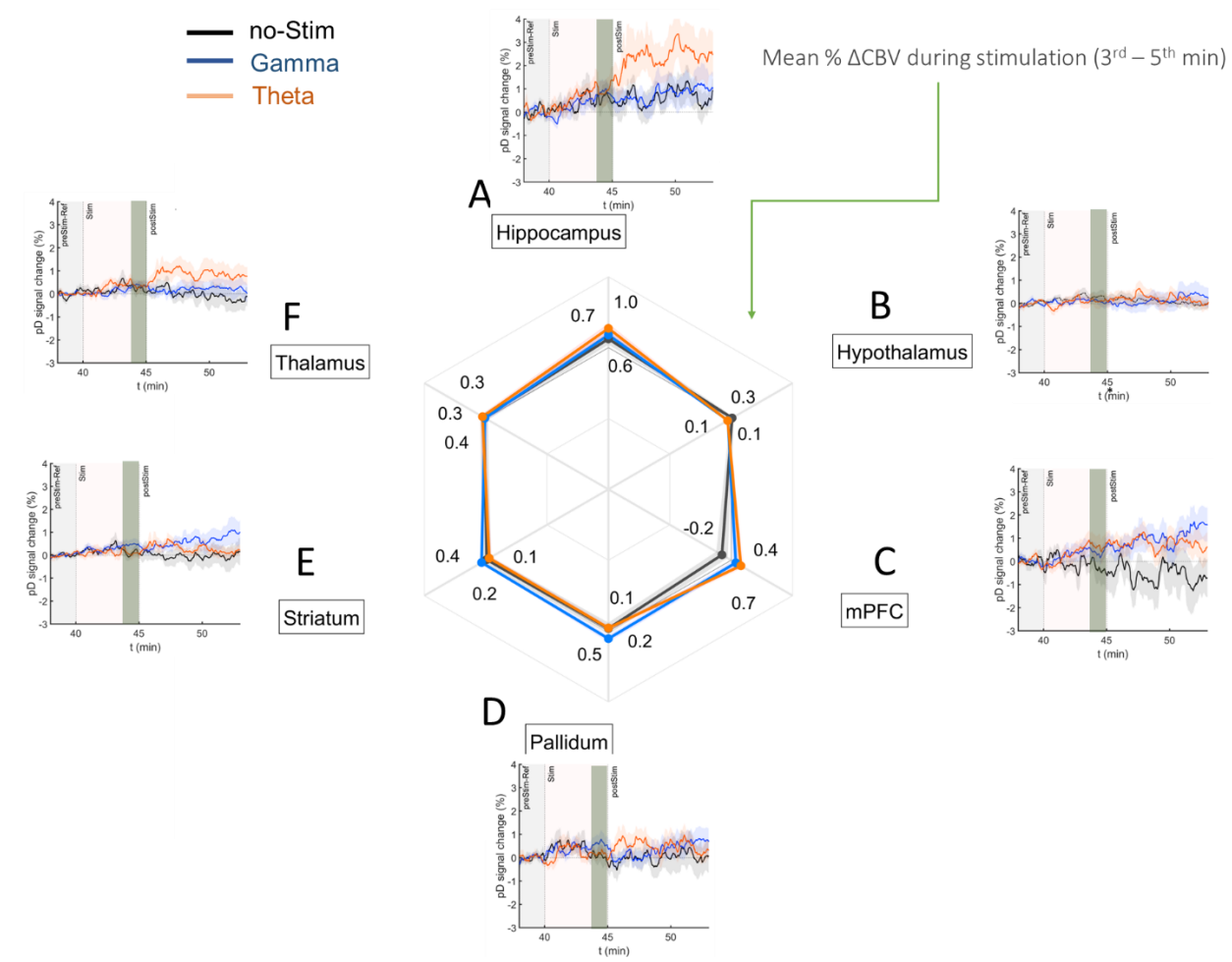

Figure 5. DBS ERA curves after stimulation onset and mean ΔCBVs in saline mice *during* the last 2 minutes of stimulation period. A – F) Temporal course (theta [orange], gamma [blue], no-stimulation [black]) of mean ΔCBV relative to baseline (2 minutes average pD signal prior to DBS) for the A) hippocampus, B) hypothalamus, C) mPFC, D) pallidum, E) striatum, and F) thalamus regions in the saline-treated animals. Radar chart insert gives the mean percentage ΔCBVs during stimulation for theta [orange], gamma [blue], and no-stimulation [dark gray] animals in the ROIs investigated. Means were calculated utilizing the last 2 minutes of pD

signals acquired during stimulation (3rd – 5th minute after stimulation onset) across animals in each stimulation category.

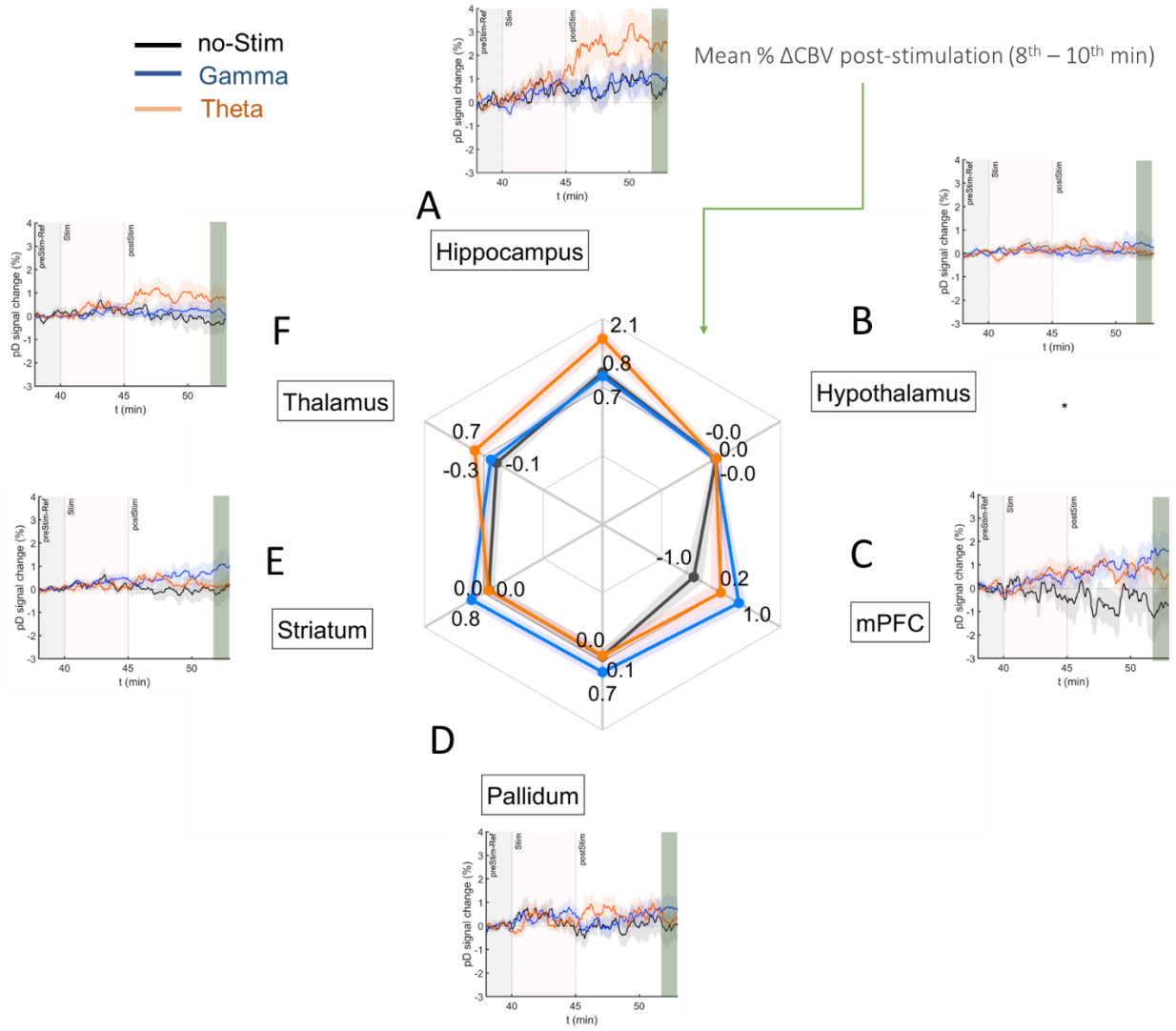

Figure 6. DBS ERA curves after stimulation onset and mean ΔCBVs in saline mice *during* the last 2 minutes of recordings in the post-stimulation period in 6 ROIs. Similar to Figure 5, but the radar chart gives the mean percentage ΔCBVs during post-stimulation for theta [orange], gamma [blue], and no-stimulation [dark

gray] for the A) hippocampus, B) hypothalamus, C) mPFC, D) pallidum, E) striatum, and F) thalamus regions in the saline-treated animals. Means were calculated utilizing the last 2 minutes of pD signals acquired post stimulation (8th – 10th minute after stimulation offset) across animals in each stimulation category.

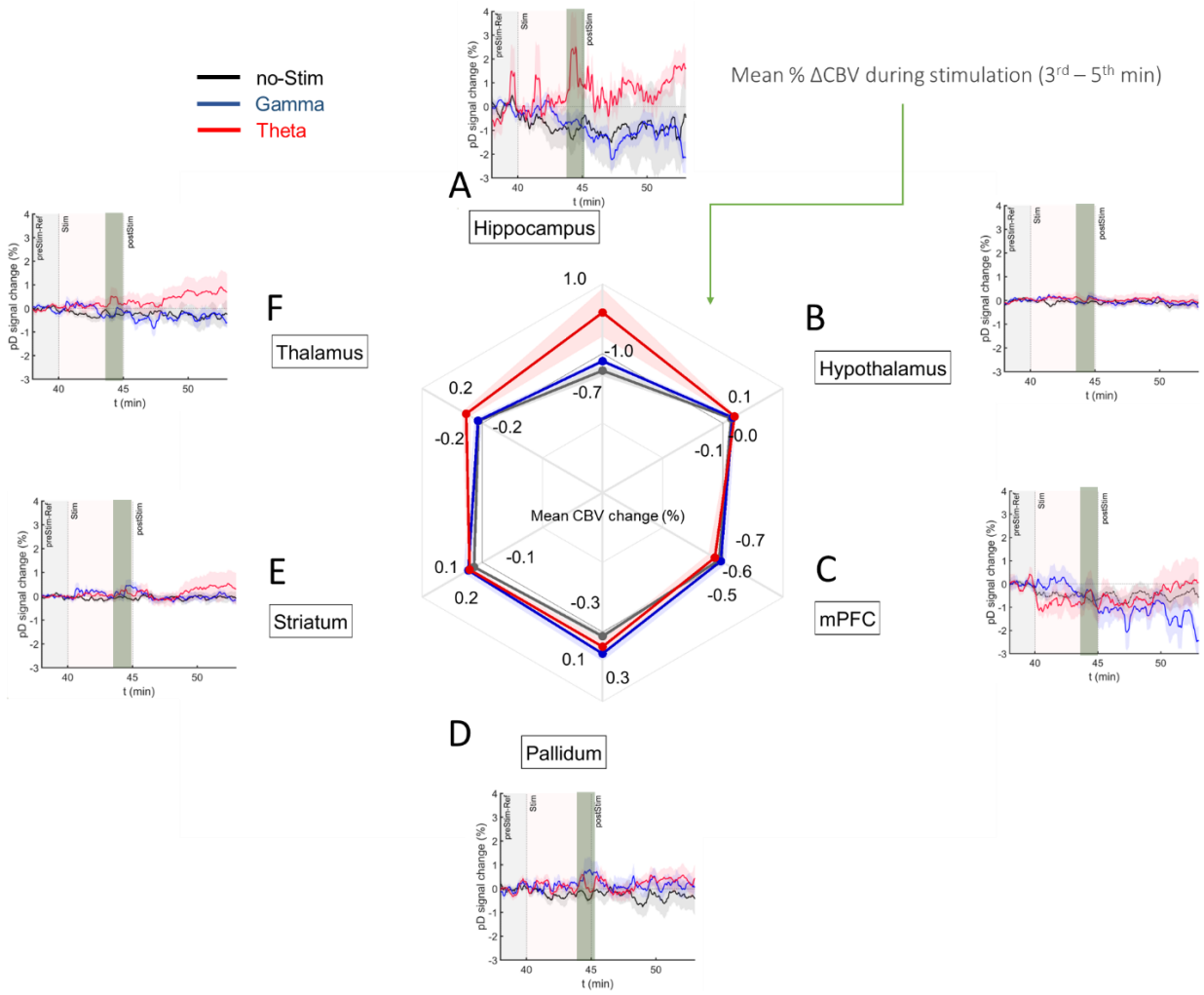

Figure 7. DBS ERA curves after stimulation onset and mean ΔCBVs in MK-801 treated mice *during* the last 2 minutes of stimulation period A – F) Temporal

course (theta [red], gamma [blue], no-stimulation [black]) of mean ΔCBV relative to baseline (2 minutes average pD signal prior to DBS) for A) hippocampus, B) hypothalamus, C) mPFC, D) pallidum, E) striatum, and F) thalamus regions in the MK-801 drug injected mice. Radar chart insert gives the mean percentage ΔCBVs during stimulation for theta [red], gamma [blue], and no-stimulation [dark gray] animals in the ROIs investigated. Means were calculated utilizing the last 2 minutes of pD signals acquired during stimulation (3rd – 5th minute after stimulation onset) across animals in each stimulation category.

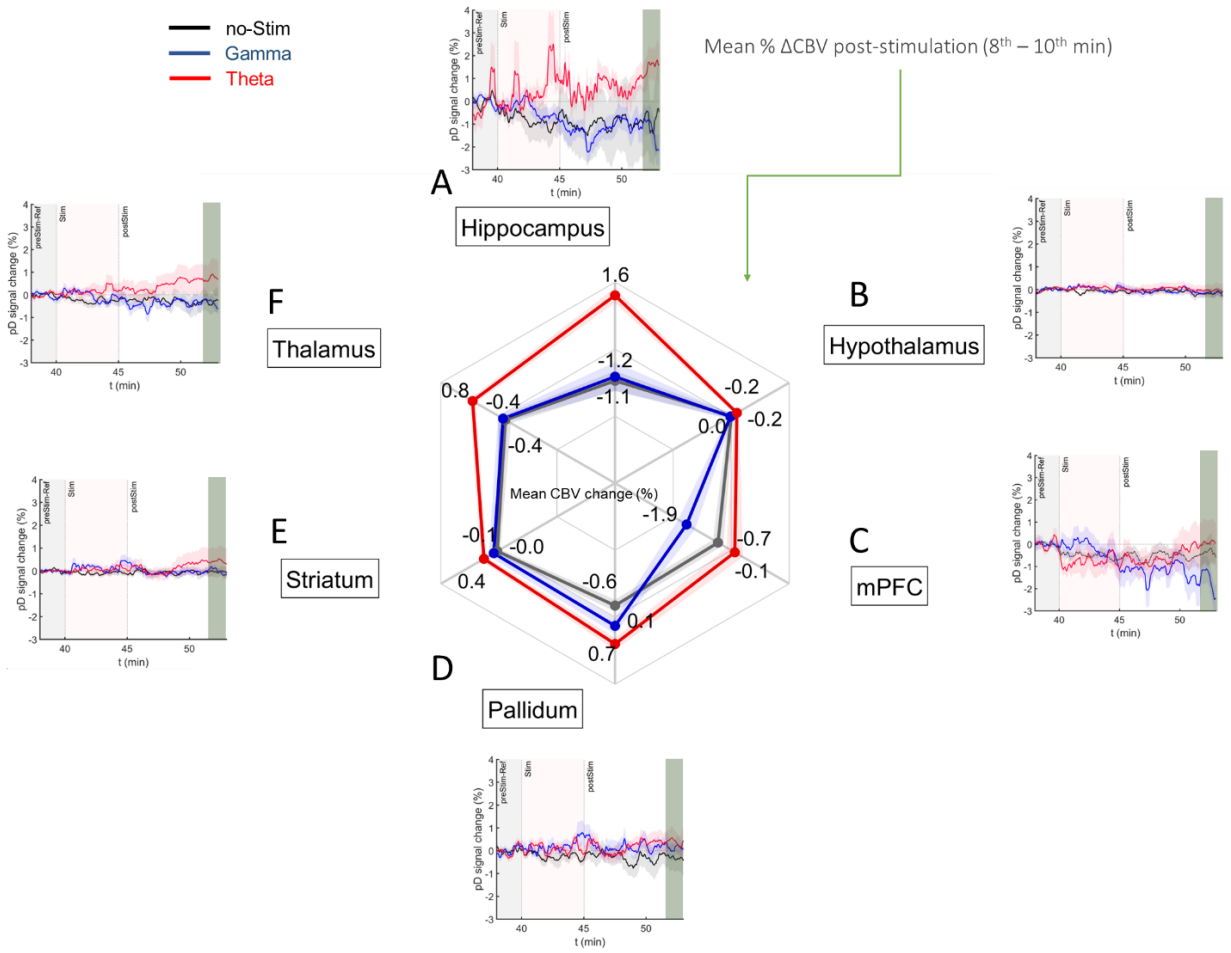

Figure 8. DBS ERA curves after stimulation onset and mean ΔCBVs in MK-801 treated mice *during* the last 2 minutes of recordings in the post-stimulation period. Similar to Figure 7, but the radar chart gives the mean percentage ΔCBVs in post-stimulation period for theta [red], gamma [blue], and no-stimulation [dark gray] for the A) hippocampus, B) hypothalamus, C) mPFC, D) pallidum, E) striatum, and F) thalamus regions in the MK-801 treated animals. Means were calculated utilizing the last 2 minutes of pD signals acquired post stimulation (8th – 10th minute after stimulation offset) across animals in each stimulation category.

Discussion

The present study utilized the high spatiotemporal resolution and sensitivity of fUSI to demonstrate that acute administration of MK-801 causes a significant reduction in CBV across all ROIs. Furthermore, we demonstrated that theta frequency MSN DBS alters regions within the septohippocampal network, with the strongest effect on the hippocampus. Intriguingly, the observed increase in hippocampal CBV remain even after cessation of DBS. On the other hand, structures outside the septohippocampal network, such as the hypothalamus and striatum, show less of a response to DBS. These effects were less pronounced with gamma frequency stimulation with very small effects on the hippocampus. These findings suggest that MSN theta frequency DBS can deliver precise neuromodulation to cognitive networks [27].

MK-801 reduced CBV in all ROIs

MK-801 and other NMDA antagonists have been widely used in preclinical models to mimic the behavioral and electrophysiological deficits associated with schizophrenia [16,18,38,39]. However, the regionally specific effects of MK-801 on CBV in such models is not well known. We observed that MK-801 reduced CBV across all ROIs. Importantly, previous fMRI studies have observed reduced BOLD signals in hippocampal and prefrontal areas in schizophrenia patients [40–42]. In this context, our findings support the use of MK-801 as a neurovascular model of schizophrenia. Furthermore, our study demonstrates the feasibility of using fUSI to identify network-

specific hemodynamic changes as an additional modality for studying neurocognitive disorders.

MSN theta stimulation was relatively specific to cognitive networks.

We observed that theta frequency MSN DBS resulted in an increase to CBV in the hippocampus in both the saline- and MK-801-treated animals. Importantly, this effect was greatest in the hippocampus, which receives direct projections from the MSN, and is a primary target for neuromodulatory interventions to treat memory dysfunction [23–25,27]. In saline control animals, significant increases to CBV were also observed in the mPFC (during and after stimulation) and thalamus (after stimulation), both of which play important roles in memory function and receive direct projections from the MSN (Fig. 1A) [22]. Interestingly, gamma stimulation did not alter hippocampal CBV, but did increase regions of the brain that were anatomically closer to the MSN. Specifically, mPFC CBV was increased in saline- treated animals, while the pallidum and striatum were increased to a lesser degree in MK-801-treated animals. This suggests that MSN gamma stimulation may have a local response to stimulation but is less specific to the neural circuitry being stimulated.

MSN theta stimulation increased hippocampal CBV during and after stimulation despite NMDA antagonism.

A leading hypothesis is that reduced N-methyl-D-aspartate (NMDA) receptor-mediated glutamatergic transmission underlies psychiatric conditions involving cognitive

and memory dysfunction [16,18,38,39,43,44]. Reductions to NMDA activity either pharmacologically or through genetic manipulation have been shown to decrease theta activity, increase gamma activity and lead to deficits in spatial navigation and memory [16,17,27,45,46]. Research by our group has found that theta frequency (7.7 Hz), but not gamma frequency (100 Hz) stimulation of the MSN during the Barnes maze task improves spatial memory in rodents following pharmacological NMDA antagonism [27]. Interestingly, previous studies have also demonstrated that MSN theta stimulation prior to the task can also improve spatial memory [23]. However, the question remains open as to how MSN DBS mediates these improvements.

<u>MSN theta stimulation may drive high frequency or spiking activity via hippocampal interneurons.</u>

A number of studies utilizing various modalities in combination with fUSI have found a strong relationship between pD signal and neuronal activity [47–49]. This relationship was also true for high frequency oscillatory activity (~100Hz) but was much weaker for lower frequency oscillations [49]. This suggests that the theta-induced increases to hippocampal CBV may reflect increased hippocampal gamma or spiking activity, rather than increases to theta oscillatory activity itself. However, given that gamma band activity is often correlated with spiking activity, differentiating between changes in oscillatory dynamics and spiking activity is not possible in the present study [50].

GABAergic interneurons in the hippocampus play an important role in synchronizing hippocampal oscillatory activity. Indeed, inhibitory neurons are

hypothesized to be a primary source of dysfunction in pathologies involving NMDA dysfunction (for review see [51]) and are inhibited by NMDA-antagonists [52,53]. One possibility is that theta frequency MSN stimulation may, by briefly stimulating afferent populations at theta-frequency, act as a 'reset' and allow synchronous innervation of hippocampal interneurons that regulate the activity of glutamatergic pyramidal cells. Indeed, it has been previously shown that optogenetic stimulation of GABAergic neurons decreases spontaneous neural activity and leads to an increase in local blood flow [54]. This hypothesis is further supported by a recent study by Nunez-Elizadle and colleagues who observed that the relationship between the fUSI signal and firing rates were greatest for putative interneurons [49]. Future studies combining single unit activity and fUSI could test this hypothesis.

<u>MSN gamma stimulation did not affect hippocampal CBV.</u>

Our previous work suggests that MSN theta, but not gamma stimulation can improve spatial memory in MK-801-treated rodents [27]. While MSN theta stimulation increased hippocampal CBV during and after stimulation in MK-801-treated animals, this was not true of MSN gamma stimulation. Gamma stimulation resulted in delayed increases to mPFC CBV in saline-treated animals and had no effect on MK-801-treated animals in any of the ROIs. These results suggest that MSN gamma stimulation is not sufficient to engage hippocampal activity and highlights the importance of frequency parameters in DBS paradigms for spatial memory. This is further supported by our previous study demonstrating no improvement to spatial memory in MK-801 treated animals with MSN gamma stimulation [27].

Implications for neuromodulation

We observed that theta-frequency stimulation of the MSN increased blood perfusion in the hippocampus following cessation of the stimulus. These effects were not observed using gamma stimulation and were still present even under conditions of pharmacologic NMDA antagonism. While the current study is in anesthetized animals, futures studies will investigate these effects in awake, behaving animals to determine the relationship between ΔCBV in the septohippocampal network and measures of memory function. It is worth noting that arguably the most effective form of neuromodulation is still electroconvulsive therapy (ECT), which is performed under anesthesia and also results in increases to cerebral blood flow [55,56]. However, ECT is very non-specific, this lack of specificity may well contribute to its detrimental effect on memory [57]. Alternatively, transcranial magnetic stimulation (TMS) is most effective when applied focally to awake, alert patients [58,59]. Because DBS can combine a relatively high degree of modulation in deep structures with the spatial specificity of TMS, it is plausible that DBS may have more benefits beyond that of ECT or TMS in treating disorders of cognitive function.

References:

[1] Ranasinghe KG, Petersen C, Kudo K, Mizuiri D, Rankin KP, Rabinovici GD, et al. Reduced synchrony in alpha oscillations during life predicts post mortem neurofibrillary tangle density in early-onset and atypical Alzheimer's disease. Alzheimer's & Dementia 2021;17:2009–19. https://doi.org/10.1002/alz.12349.

[2] Tu M-C, Chung H-W, Hsu Y-H, Yang J-J, Wu W-C. Stage-Dependent Cerebral Blood Flow and Leukoaraiosis Couplings in Subcortical Ischemic Vascular Disease and Alzheimer's Disease. J Alzheimers Dis 2022;86:729–39. https://doi.org/10.3233/JAD-215405.

[3] Dougherty DD, Chou T, Corse AK, Arulpragasam AR, Widge AS, Cusin C, et al. Acute deep brain stimulation changes in regional cerebral blood flow in obsessive-compulsive disorder. J Neurosurg 2016;125:1087–93. https://doi.org/10.3171/2015.9.JNS151387.

[4] Laxton AW, Tang-Wai DF, McAndrews MP, Zumsteg D, Wennberg R, Keren R, et al. A phase I trial of deep brain stimulation of memory circuits in Alzheimer's disease. Ann Neurol 2010;68:521–34. https://doi.org/10.1002/ana.22089.

[5] Macé E, Montaldo G, Cohen I, Baulac M, Fink M, Tanter M. Functional ultrasound imaging of the brain. Nat Methods 2011;8:662–4. https://doi.org/10.1038/nmeth.1641.

[6] Mace E, Montaldo G, Osmanski B-F, Cohen I, Fink M, Tanter M. Functional ultrasound imaging of the brain: theory and basic principles. IEEE Transactions on Ultrasonics, Ferroelectrics, and Frequency Control 2013;60:492–506. https://doi.org/10.1109/TUFFC.2013.2592.

530 [7] Rabut C, Ferrier J, Bertolo A, Osmanski B, Mousset X, Pezet S, et al. Pharmaco-fUS:
531 Quantification of pharmacologically-induced dynamic changes in brain perfusion and
532 connectivity by functional ultrasound imaging in awake mice. NeuroImage
533 2020;222:117231. https://doi.org/10.1016/j.neuroimage.2020.117231.
534 [8] Norman SL, Maresca D, Christopoulos VN, Griggs WS, Demene C, Tanter M, et al. Single-
535 trial decoding of movement intentions using functional ultrasound neuroimaging. Neuron
536 2021;109:1554-1566.e4. https://doi.org/10.1016/j.neuron.2021.03.003.
537 [9] Uhlhaas PJ, Singer W. Abnormal neural oscillations and synchrony in schizophrenia. Nature
538 Reviews Neuroscience 2010;11:100–13. https://doi.org/10.1038/nrn2774.
539 [10] Barr MS, Rajji TK, Zomorrodi R, Radhu N, George TP, Blumberger DM, et al. Impaired
540 theta-gamma coupling during working memory performance in schizophrenia.
541 Schizophrenia Research 2017;189:104–10. https://doi.org/10.1016/j.schres.2017.01.044.
542 [11] Jafari Z, Kolb BE, Mohajerani MH. Neural oscillations and brain stimulation in Alzheimer's
543 disease. Prog Neurobiol 2020;194:101878.
544 https://doi.org/10.1016/j.pneurobio.2020.101878.
545 [12] Gonzalez-Burgos G, Lewis DA. NMDA Receptor Hypofunction, Parvalbumin-Positive
546 Neurons, and Cortical Gamma Oscillations in Schizophrenia. Schizophrenia Bulletin
547 2012;38:950–7. https://doi.org/10.1093/schbul/sbs010.
548 [13] Gu Z, Alexander GM, Dudek SM, Yakel JL. Hippocampus and Entorhinal Cortex Recruit
549 Cholinergic and NMDA Receptors Separately to Generate Hippocampal Theta Oscillations.
550 Cell Reports 2017;21:3585–95. https://doi.org/10.1016/j.celrep.2017.11.080.

551 [14] Collingridge G. The role of NMDA receptors in learning and memory. Nature
552 1987;330:604–5. https://doi.org/10.1038/330604a0.
553 [15] Spangler EL, Bresnahan EL, Garofalo P, Muth NJ, Heller B, Ingram DK. NMDA receptor
554 channel antagonism by dizocilpine (MK-801) impairs performance of rats in aversively
555 motivated complex maze tasks. Pharmacol Biochem Behav 1991;40:949–58.
556 https://doi.org/10.1016/0091-3057(91)90111-e.
557 [16] Newcomer JW, Farber NB, Jevtovic-Todorovic V, Selke G, Melson AK, Hershey T, et al.
558 Ketamine-Induced NMDA Receptor Hypofunction as a Model of Memory Impairment and
559 Psychosis. Neuropsychopharmacology 1999;20:106–18. https://doi.org/10.1016/S0893-
560 133X(98)00067-0.
561 [17] Korotkova T, Fuchs EC, Ponomarenko A, von Engelhardt J, Monyer H. NMDA receptor
562 ablation on parvalbumin-positive interneurons impairs hippocampal synchrony, spatial
563 representations, and working memory. Neuron 2010;68:557–69.
564 https://doi.org/10.1016/j.neuron.2010.09.017.
565 [18] Saunders JA, Gandal MJ, Siegel SJ. NMDA antagonists recreate signal-to-noise ratio and
566 timing perturbations present in schizophrenia. Neurobiology of Disease 2012;46:93–100.
567 https://doi.org/10.1016/J.NBD.2011.12.049.
568 [19] Billingslea EN, Tatard-Leitman VM, Anguiano J, Jutzeler CR, Suh J, Saunders JA, et al.
569 Parvalbumin Cell Ablation of NMDA-R1 Causes Increased Resting Network Excitability with
570 Associated Social and Self-Care Deficits. Neuropsychopharmacol 2014;39:1603–13.
571 https://doi.org/10.1038/npp.2014.7.

572 [20] Fuhrmann F, Justus D, Sosulina L, Kaneko H, Beutel T, Friedrichs D, et al. Locomotion,
573 Theta Oscillations, and the Speed-Correlated Firing of Hippocampal Neurons Are
574 Controlled by a Medial Septal Glutamatergic Circuit. Neuron 2015;86:1253–64.
575 https://doi.org/10.1016/j.neuron.2015.05.001.
576 [21] Leão RN, Targino ZH, Colom LV, Fisahn A. Interconnection and synchronization of neuronal
577 populations in the mouse medial septum/diagonal band of Broca. Journal of
578 Neurophysiology 2015;113:971–80. https://doi.org/10.1152/jn.00367.2014.
579 [22] Takeuchi Y, Nagy AJ, Barcsai L, Li Q, Ohsawa M, Mizuseki K, et al. The Medial Septum as a
580 Potential Target for Treating Brain Disorders Associated With Oscillopathies. Frontiers in
581 Neural Circuits 2021;15.
582 [23] Lee DJ, Gurkoff GG, Izadi A, Berman RF, Ekstrom AD, Muizelaar JP, et al. Medial Septal
583 Nucleus Theta Frequency Deep Brain Stimulation Improves Spatial Working Memory after
584 Traumatic Brain Injury. Journal of Neurotrauma 2013;30:131–9.
585 https://doi.org/10.1089/neu.2012.2646.
586 [24] Lee DJ, Gurkoff GG, Izadi A, Seidl SE, Echeverri A, Melnik M, et al. Septohippocampal
587 Neuromodulation Improves Cognition after Traumatic Brain Injury. Journal of
588 Neurotrauma 2015;32:1822–32. https://doi.org/10.1089/neu.2014.3744.
589 [25] Lee DJ, Izadi A, Melnik M, Seidl S, Echeverri A, Shahlaie K, et al. Stimulation of the medial
590 septum improves performance in spatial learning following pilocarpine-induced status
591 epilepticus. Epilepsy Research 2017;130:53–63.
592 https://doi.org/10.1016/j.eplepsyres.2017.01.005.

593 [26] Cole ER, Grogan DP, Laxpati NG, Fernandez AM, Skelton HM, Isbaine F, et al. Evidence
594 supporting deep brain stimulation of the medial septum in the treatment of temporal lobe
595 epilepsy. Epilepsia 2022;63:2192–213. https://doi.org/10.1111/epi.17326.
596 [27] Zepeda NC, Crown LM, Medvidovic S, Choi W, Sheth M, Bergosh M, et al. Frequency-
597 specific medial septal nucleus deep brain stimulation improves spatial memory in MK-801-
598 treated male rats. Neurobiology of Disease 2022;170:105756.
599 https://doi.org/10.1016/j.nbd.2022.105756.
600 [28] Grubbs FE. Procedures for Detecting Outlying Observations in Samples. Technometrics
601 1969;11:1–21. https://doi.org/10.1080/00401706.1969.10490657.
602 [29] Stefansky W. Rejecting Outliers in Factorial Designs. Technometrics 1972;14:469–79.
603 https://doi.org/10.2307/1267436.
604 [30] Wegener N, Nagel J, Gross R, Chambon C, Greco S, Pietraszek M, et al. Evaluation of brain
605 pharmacokinetics of (+)MK-801 in relation to behaviour. Neurosci Lett 2011;503:68–72.
606 https://doi.org/10.1016/j.neulet.2011.08.012.
607 [31] Wang Q, Ding S-L, Li Y, Royall J, Feng D, Lesnar P, et al. The Allen Mouse Brain Common
608 Coordinate Framework: A 3D Reference Atlas. Cell 2020;181:936-953.e20.
609 https://doi.org/10.1016/j.cell.2020.04.007.
610 [32] Ledoux LA, Brands PJ, Hoeks AP. Reduction of the clutter component in Doppler
611 ultrasound signals based on singular value decomposition: a simulation study. Ultrason
612 Imaging 1997;19:1–18. https://doi.org/10.1177/016173469701900101.

613 [33] Stringer C, Pachitariu M. Computational processing of neural recordings from calcium
614 imaging data. Current Opinion in Neurobiology 2019;55:22–31.
615 https://doi.org/10.1016/j.conb.2018.11.005.
616 [34] Friedrich J, Giovannucci A, Pnevmatikakis EA. Online analysis of microendoscopic 1-photon
617 calcium imaging data streams. PLOS Computational Biology 2021;17:e1008565.
618 https://doi.org/10.1371/journal.pcbi.1008565.
619 [35] Pnevmatikakis EA, Giovannucci A. NoRMCorre: An online algorithm for piecewise rigid
620 motion correction of calcium imaging data. Journal of Neuroscience Methods
621 2017;291:83–94. https://doi.org/10.1016/j.jneumeth.2017.07.031.
622 [36] Liu XS. Statistical Power Analysis for the Social and Behavioral Sciences: Basic and
623 Advanced Techniques. Routledge; 2013.
624 [37] Gómez-de-Mariscal E, Guerrero V, Sneider A, Jayatilaka H, Phillip JM, Wirtz D, et al. Use of
625 the p-values as a size-dependent function to address practical differences when analyzing
626 large datasets. Sci Rep 2021;11:20942. https://doi.org/10.1038/s41598-021-00199-5.
627 [38] Balu DT. The NMDA Receptor and Schizophrenia: From Pathophysiology to Treatment. Adv
628 Pharmacol 2016;76:351–82. https://doi.org/10.1016/bs.apha.2016.01.006.
629 [39] Farber NB. The NMDA Receptor Hypofunction Model of Psychosis. Annals of the New York
630 Academy of Sciences 2003;1003:119–30. https://doi.org/10.1196/annals.1300.008.
631 [40] MacDonald SWS, Nyberg L, Bäckman L. Intra-individual variability in behavior: links to
632 brain structure, neurotransmission and neuronal activity. Trends in Neurosciences
633 2006;29:474–80. https://doi.org/10.1016/J.TINS.2006.06.011.

634 [41] Gur RE, Gur RC. Functional magnetic resonance imaging in schizophrenia. Dialogues in
635 Clinical Neuroscience 2010;12:333–43. https://doi.org/10.31887/DCNS.2010.12.3/rgur.
636 [42] Bedford NJ, Surguladze S, Giampietro V, Brammer MJ, David AS. Self-evaluation in
637 schizophrenia: an fMRI study with implications for the understanding of insight. BMC
638 Psychiatry 2012;12:106. https://doi.org/10.1186/1471-244X-12-106.
639 [43] Moghaddam B, Javitt D. From Revolution to Evolution: The Glutamate Hypothesis of
640 Schizophrenia and its Implication for Treatment. Neuropsychopharmacol 2012;37:4–15.
641 https://doi.org/10.1038/npp.2011.181.
642 [44] Lin C-H, Huang Y-J, Lin C-J, Lane H-Y, E. Tsai G. NMDA Neurotransmission Dysfunction in
643 Mild Cognitive Impairment and Alzheimer's Disease. Current Pharmaceutical Design
644 2014;20:5169–79.
645 [45] Stark E, Eichler R, Roux L, Fujisawa S, Rotstein HG, Buzsáki G. Inhibition-induced theta
646 resonance in cortical circuits. Neuron 2013;80.
647 https://doi.org/10.1016/j.neuron.2013.09.033.
648 [46] Ward KR, Featherstone RE, Naschek MJ, Melnychenko O, Banerjee A, Yi J, et al. Src
649 deficient mice demonstrate behavioral and electrophysiological alterations relevant to
650 psychiatric and developmental disease. Progress in Neuro-Psychopharmacology and
651 Biological Psychiatry 2019;93:84–92. https://doi.org/10.1016/j.pnpbp.2019.02.017.
652 [47] Boido D, Rungta RL, Osmanski B-F, Roche M, Tsurugizawa T, Le Bihan D, et al. Mesoscopic
653 and microscopic imaging of sensory responses in the same animal. Nat Commun
654 2019;10:1110. https://doi.org/10.1038/s41467-019-09082-4.

[48] Aydin A-K, Haselden WD, Goulam Houssen Y, Pouzat C, Rungta RL, Demené C, et al. Transfer functions linking neural calcium to single voxel functional ultrasound signal. Nat Commun 2020;11:2954. https://doi.org/10.1038/s41467-020-16774-9.

[49] Nunez-Elizalde AO, Krumin M, Reddy CB, Montaldo G, Urban A, Harris KD, et al. Neural correlates of blood flow measured by ultrasound. Neuron 2022;110:1631-1640.e4. https://doi.org/10.1016/j.neuron.2022.02.012.

[50] Buzsáki G, Schomburg EW. What does gamma coherence tell us about inter-regional neural communication? Nat Neurosci 2015;18:484–9. https://doi.org/10.1038/nn.3952.

[51] Marín O. Interneuron dysfunction in psychiatric disorders. Nat Rev Neurosci 2012;13:107–20. https://doi.org/10.1038/nrn3155.

[52] Homayoun H, Moghaddam B. NMDA receptor hypofunction produces opposite effects on prefrontal cortex interneurons and pyramidal neurons. J Neurosci 2007;27:11496–500. https://doi.org/10.1523/JNEUROSCI.2213-07.2007.

[53] Cohen SM, Tsien RW, Goff DC, Halassa MM. The impact of NMDA Receptor hypofunction on GABAergic interneurons in the pathophysiology of schizophrenia. Schizophr Res 2015;167:98–107. https://doi.org/10.1016/j.schres.2014.12.026.

[54] Anenberg E, Chan AW, Xie Y, LeDue JM, Murphy TH. Optogenetic Stimulation of GABA Neurons can Decrease Local Neuronal Activity While Increasing Cortical Blood Flow. J Cereb Blood Flow Metab 2015;35:1579–86. https://doi.org/10.1038/jcbfm.2015.140.

[55] Espinoza RT, Kellner CH. Electroconvulsive Therapy. New England Journal of Medicine 2022;386:667–72. https://doi.org/10.1056/NEJMra2034954.

676 [56] Singh A, Kar SK. How Electroconvulsive Therapy Works?: Understanding the
677 Neurobiological Mechanisms. Clinical Psychopharmacology and Neuroscience
678 2017;15:210–21. https://doi.org/10.9758/cpn.2017.15.3.210.
679 [57] Andrade C, Arumugham SS, Thirthalli J. Adverse Effects of Electroconvulsive Therapy.
680 Psychiatric Clinics 2016;39:513–30. https://doi.org/10.1016/j.psc.2016.04.004.
681 [58] Gersner R, Kravetz E, Feil J, Pell G, Zangen A. Long-Term Effects of Repetitive Transcranial
682 Magnetic Stimulation on Markers for Neuroplasticity: Differential Outcomes in
683 Anesthetized and Awake Animals. J Neurosci 2011;31:7521–6.
684 https://doi.org/10.1523/JNEUROSCI.6751-10.2011.
685 [59] Xu T, Sturgeon D, Ramirez JSB, Froudist-Walsh S, Margulies DS, Schroeder CE, et al.
686 Interindividual Variability of Functional Connectivity in Awake and Anesthetized Rhesus
687 Macaque Monkeys. Biological Psychiatry: Cognitive Neuroscience and Neuroimaging
688 2019;4:543–53. https://doi.org/10.1016/j.bpsc.2019.02.005.
689
690
691
692
693